Kinetics of the IO Radical. 1. Reaction of IO with ClO

Andrew A. Turnipseed,† Mary K. Gilles, James B. Burkholder, and A. R. Ravishankara*

Aeronomy Laboratory, National Oceanic and Atmospheric Administration, Boulder, Colorado 80303, and Cooperative Institute for Research in Environmental Sciences, University of Colorado, Boulder, Colorado 80309

Received: March 12, 1997; In Final Form: May 9, 1997[⊗]

The rate coefficient for the IO + ClO → products (5) reaction was measured by coupling discharge flow and pulsed laser-induced fluorescence techniques. Rate coefficients were measured from 200 to 362 K by monitoring the temporal profile of IO in an excess of ClO. The rate coefficient is described by the expression: $k_5(T) = (5.1 \pm 1.7) \times 10^{-12} \exp[(280 \pm 80)/T]$ cm^3 molecule^{-1} s^{-1} where the quoted uncertainties include estimated systematic errors. Atomic iodine was identified as a major product of reaction 5. A branching ratio of $\Phi = 0.14 \pm 0.04$ at 298 K was obtained for the sum of channels which do not produce I atoms.

Introduction

The reactivity of chlorine- and bromine-containing radicals are of interest in atmospheric chemistry due to their ability to catalytically destroy stratospheric ozone. However, iodine-containing radicals have received much less attention. It is known that the oceans are a significant source of iodine to the atmosphere, primarily in the form of CH_3I.[1−3] The possible role of iodine in tropospheric chemistry, and in particular, the marine boundary layer, has been described previously.[4,5] More recently, halogen chemistry has been implicated in the sporadic rapid ozone loss observed in the Arctic spring after sunrise.[6,7] Iodine may lead to catalytic ozone depletion via the reaction sequence

$$I + O_3 \rightarrow IO + O_2 \quad (1)$$

$$X + O_3 \rightarrow XO + O_2 \quad (2)$$

$$IO + XO \rightarrow\rightarrow I + X + O_2 \quad (3)$$

$$\text{net: } 2O_3 \rightarrow 3O_2 \quad (4)$$

where X represents Cl, Br, I, or OH. Reaction 3 is denoted with a double arrow to indicate that it may proceed by more than one elementary step. Because reaction 3 is the rate-limiting step in this sequence, the rate coefficients for these reactions must be known to ascertain the effectiveness of these cycles.

Solomon *et al.*[8] recently reevaluated the possible role of iodine in the catalytic destruction of stratospheric ozone. Previously it was assumed that iodine could play a significant role only in tropospheric chemistry, due to the short tropospheric photolysis lifetime of iodine-containing compounds.[4,5] However, Solomon *et al.*[8] postulated that iodine-containing compounds can be rapidly transported to the stratosphere by strong convective transport in the tropics. Once in the stratosphere, these compounds would readily photolyze to release I atoms which then catalytically destroy ozone via reactions 1−3. Since the reservoir species for iodine in the atmosphere (i.e., HI, HOI, or $IONO_2$) are photolytically unstable, most of the atmospheric iodine will be in the active forms of I or IO. Therefore, iodine is particularly effective at destroying ozone, and small amounts of iodine can make a significant contribution to ozone loss at low altitudes.

Solomon *et al.*[8] pointed out that the trend in low-altitude, midlatitude ozone loss observed over the last decade could be explained by the presence of small concentrations of iodine (≤1 pptv) interacting with chlorine and bromine. This trend could reflect the increasing chlorine abundance in the stratosphere over this time period. If all of this ozone depletion is attributed to the IO + ClO cycle, the rate coefficient for the reaction

$$IO + ClO \rightarrow \text{products} \quad (5)$$

has to be large (≈10^{-10} cm^3 molecule^{-1} s^{-1}), the reaction products need to be atomic iodine and chlorine or lead to them in the atmosphere, and the stratospheric abundance of iodine has to be ∼1 pptv. Lower values of iodine and/or the rate coefficient, k_5, will lead to a proportionately smaller contribution to ozone depletion.

The chemistry of iodine also merits concern due to the possible anthropogenic emissions of iodine-containing compounds. If a significant fraction of these compounds reach the stratosphere, either by rapid transport or by direct release into the upper atmosphere, then the effectiveness of their interaction with chlorine or bromine in ozone destruction must be known. For example, when the ozone depletion potential of a compound such as CF_3I is evaluated, the reactions of iodine need to be considered.

We have used pulsed laser photolysis/pulsed laser-induced fluorescence (LP-PLIF) to produce and monitor IO radicals. We have combined a discharge flow source for producing ClO radicals with UV absorption for determining [ClO] to measure the rate coefficient for reaction 5 over the temperature range important in the atmosphere. The I atom yield in reaction 5 was also determined. In the second part of our study we have measured the IO + BrO reaction rate coefficient and discuss the atmospheric implications of the kinetic measurements.

Experimental Section

Measurement of rate coefficients for a bimolecular reaction under pseudo-first-order conditions requires that the concentration of one reagent be constant and known. The easiest way to attain this requirement is to have a large excess of one reagent over the other. First-order kinetics has the advantage that only the absolute concentration of the excess reagent is needed to determine the rate coefficient. The accuracy of the measured rate constant is directly related to the accuracy with which the

* Address correspondence to this author at: NOAA/ERL, R/E/AL2, 325 Broadway, Boulder, CO 80303. Also affiliated with the Department of Chemistry and Biochemistry, University of Colorado, Boulder, CO 80309.

† Current address: Department of Biology (EPOB), University of Colorado, Boulder, CO 80309.

⊗ Abstract published in *Advance ACS Abstracts,* July 1, 1997.

S1089-5639(97)00914-6 CCC: $14.00

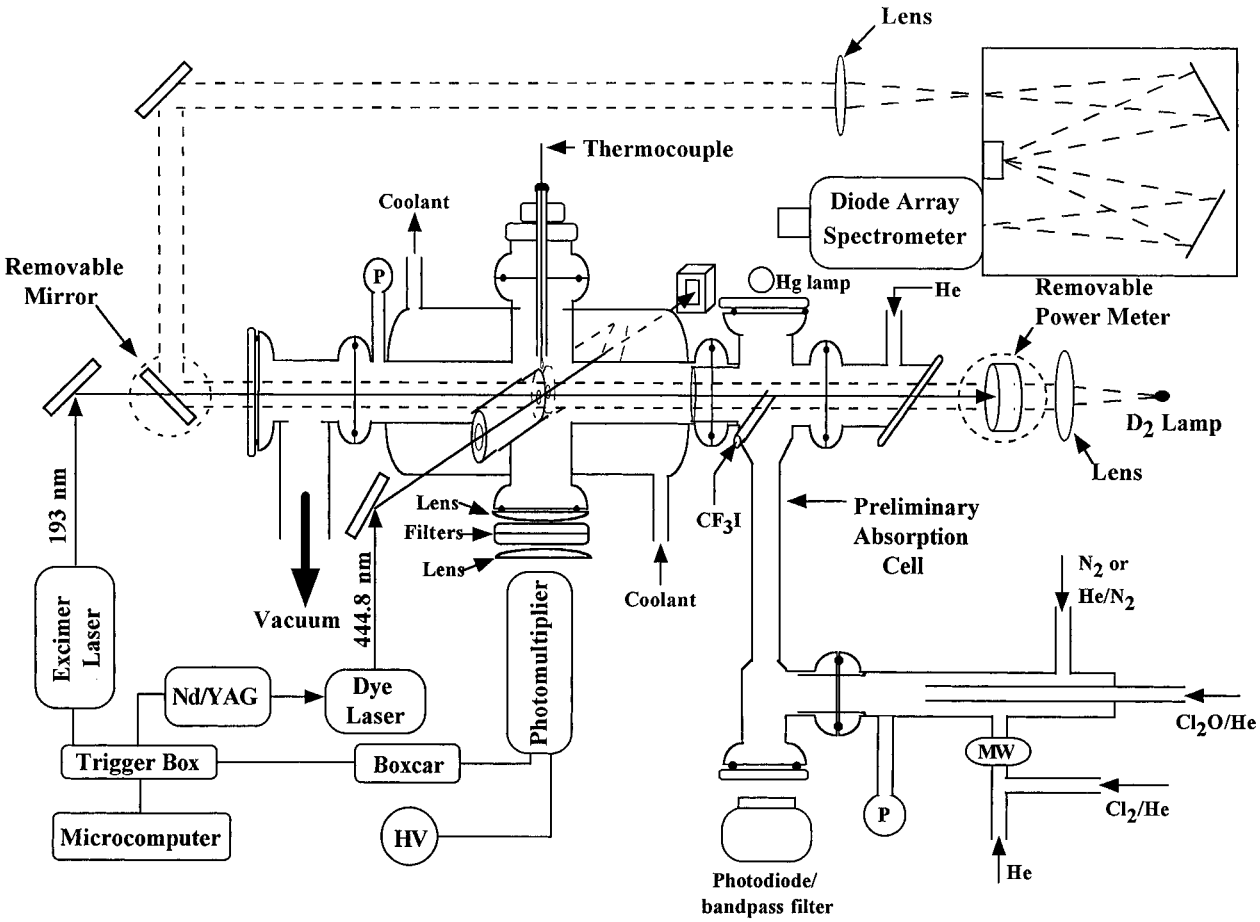

Figure 1. Schematic of the pulsed laser photolysis/pulsed laser-induced fluorescence system coupled to a discharge flow system for generating ClO radicals (P = capacitance monometer, MW = microwave, HV = high voltage).

excess reagent concentration is measured. In a conventional pulsed photolysis system, the excess reagent is usually a stable gas whose concentration is measured using flow rates and pressure or UV absorption. However, to study the reaction of IO + ClO under pseudo-first-order conditions, one of the unstable radical species must be generated in large excess, its concentration must be measured, and any of its losses due to reactions (i.e., self-reaction) must be quantified. In addition, the temporal profile of the other radical must be measured. Due to the slow self-reaction[9] of ClO and the sensitivity with which IO can be detected by laser-induced fluorescence,[10] we chose to study this reaction under conditions of $[ClO] > 10[IO]_0$ (pseudo-first-order in IO). The experimental apparatus (Figure 1) combines discharge flow (DF), pulsed laser photolysis/pulsed laser-induced fluorescence (PLP/PLIF), and UV absorption spectroscopy. The merging of techniques which are normally optimized under very different experimental conditions (i.e., pressure, flow rate, and velocity) leads to some complications that are not normally encountered (for example, temperature gradients and fast loss due to transport from the viewing zone). These complications and their influence on the measurements are addressed in the following sections.

ClO Generation. The flow tube consisted of a 2.54 cm Pyrex tube held at 298 K with a movable injector (0.6 cm o.d.) down the center of the tube. Typically a large flow of N_2 or He/N_2 was added such that the flow rate was 13−60 STP cm^3 s^{-1}, total pressure was 5−16 Torr, and linear gas flow velocity was $v = 500-1000$ cm s^{-1} in the flow tube. Cl atoms were generated in a side arm of the flow tube by passing a dilute (0.1−1% Cl_2) mixture of Cl_2 in He through a microwave discharge. Within the flow tube, Cl atoms reacted with either Cl_2O, OClO, or O_3 which were added through the movable injector.

$$Cl + Cl_2O \rightarrow ClO + Cl_2 \quad (6)$$

$$Cl + OClO \rightarrow 2ClO \quad (7)$$

$$Cl + O_3 \rightarrow ClO + O_2 \quad (8)$$

Concentrations of Cl_2O, OClO, or O_3 were always sufficiently large to react away any Cl atoms, which avoided removal of IO or its precursors via their reactions with Cl atoms. The residence time within the flow tube was ∼15 ms, which was sufficient for complete consumption of the Cl atoms. However, since ClO concentrations were typically $<10^{14}$ molecule cm^{-3}, little ClO was lost due to its self-reaction:

$$ClO + ClO \rightarrow ClOO + Cl \quad (9a)$$

$$\rightarrow Cl_2 + O_2 \quad (9b)$$

$$\rightarrow OClO + Cl \quad (9c)$$

$$\xrightarrow{M} Cl_2O_2 \quad (9d)$$

where $k_9(298\ K) = 2 \times 10^{-14}$ cm^3 $molecule^{-1}$ s^{-1} at 5 Torr.[9] It should also be noted that channels 9a and 9c produce Cl atoms which were recycled rapidly to ClO by reaction with the excess Cl_2O, OClO or O_3. Thus, not all of reaction 9 leads to ClO removal, and the loss was quite small.

From the flow tube, the gases passed through a narrow (1.3 cm i.d.) 50 cm preliminary absorption cell held at 298 K. This

cell was used to calibrate the path length of the photolysis cell as described below. The residence time within the preliminary absorption cell was ~20 ms.

UV Absorption Spectroscopy. The gas effluent from the preliminary absorption cell passed into the photolysis cell which consisted of an 18 cm long jacketed Pyrex tube (2.0 cm i.d.) with orthogonal windows in the center. ClO concentrations were measured through the photolysis cell via UV absorption spectroscopy. The output of a D_2 lamp was collimated and passed through the photolysis cell along the axis of the flow (counter to the path of the photolysis laser). The beam was then focused onto the entrance slit of a 0.5 m spectrometer. The spectrometer employed a 300 grooves/mm grating and a cooled 1024 element diode array detector, which allowed measurements over a 165 nm wide region. The ClO concentration was quantified using the unstructured portion of the spectrum since the cross section in this region is known to be independent of temperature and resolution.[11] The spectral subtraction, however, utilized the structured region of the spectrum. A slit width of 150 μm resulted in a spectral resolution of 0.8 nm (fwhm). For monitoring ClO, OClO, and Cl_2O, the spectrometer was typically set to observe from 220 to 385 nm. This wavelength range was calibrated using the emission lines from a low-pressure Hg lamp. Reference spectra of ClO and OClO needed for spectral subtraction were measured using the same spectrometer.

As seen in Figure 1, only part of the optical path was at the temperature of interest. Also, to minimize the formation of solid deposits on the entrance and exit windows, pure He or N_2 was flushed in front of the windows, slightly reducing the optical path length. Therefore, it was necessary to measure the "effective" absorption path length through the photolysis cell under each set of experimental conditions (flows, pressure, temperature). In the simplest case, the path length can be divided into two regions: (1) the temperature-controlled region at temperature T and (2) the 298 K region, the sections before and after the photolysis cell. The temperature gradients at the entrance and exit of the temperature-controlled region were measured using a movable thermocouple probe and compensated for each other. The absorption due to ClO measured through the photolysis cell was

$$A_{tot} = A_T + A_{298} = \sigma_T L_T [ClO]_T + \sigma_{298} L_{298} [ClO]_{298} \quad (I)$$

where $A_{tot} = -\ln (I/I_0)$ (I being the light intensity with ClO present and I_0 when it is not) and σ is the absorption cross section. L_T and L_{298} are the path lengths at temperatures T and 298 K, respectively. Knowing that $[ClO]_T = [ClO]_{298}(298\ K/T)$ and that σ at 253.7 nm is temperature independent, $[ClO]_T$ was described by

$$[ClO]_T = \frac{A_{tot}}{\sigma L_{eff}} \quad (II)$$

where $L_{eff} = L_{298}(T/298) + L_T$. L_{eff} was measured prior to each experiment by adding O_3 to the flow tube and measuring its absorption at 253.7 nm (Hg line) in the preliminary absorption cell (all at 298 K). The O_3 then passed through the LIF reactor where its absorption was again measured by the D_2 lamp/diode array spectrometer at the same wavelength. O_3 was chosen as our standard since it is known that its absorption cross section at 253.7 nm ($\sigma = 1.16 \times 10^{-17}$ cm^2 molecule^{-1}) does not significantly change with temperature (<2% change from 298 to 200 K).[12] The ratio of the absorptions in the two cells was used to calculate L_{eff}.

$$\frac{A_{tot}}{A_{Hg}}\left(\frac{T}{298}\right) = \frac{L_{eff}}{L_{Hg}} \quad (III)$$

where A_{Hg} and L_{Hg} are, respectively, the measured absorption (using the Hg lamp) and the path length (50 cm) for the preliminary absorption cell.

Reference spectra for the species measured in the present study are shown in Figure 2a and are in good agreement with those in the literature.[9,13] ClO reference spectra were measured prior to each experiment by titrating either OClO, O_3, or Cl_2O with an excess of Cl atoms (reaction 6, 7, or 8). These reference spectra were recorded under flow, pressure, and temperature conditions that were identical to the subsequent kinetic experiments. In contrast to the reference spectral measurements, in the kinetics experiment, ClO was produced in an excess of Cl_2O, OClO (OClO was used only at 298 K), or O_3 (which was used only for the I atom yield experiments). The ClO concentration was measured after generating IO and measuring its temporal profile using the PLP/PLIF (described below). The photolysis laser was blocked, and the D_2 beam was passed through the photolysis cell to measure the ClO/Cl_2O, ClO/OClO, or ClO/O_3 spectrum. I_0 for this measurement was obtained after turning off the microwave discharge and shutting off the flow of Cl_2O, OClO, or O_3. The absorption due to ClO was extracted from the measured spectrum by subtracting the scaled ClO reference spectrum until all of the ClO structured absorption was completely removed. An example of this subtraction using Cl_2O is shown in Figure 2b, and the residual is shown in Figure 2c. The abundance of ClO subtracted to get the unstructured residual was used to determine the [ClO] by using the absorption at 253.7 nm ($A_{tot} = L_{eff}\sigma[ClO]_T$, $\sigma = 4.25 \times 10^{-18}$ cm^2 molecule^{-1}).[9]

PLP/PLIF System. IO radicals were generated in the photolysis reactor following the 193 nm photolysis of N_2O/CF_3I or N_2O/I_2 mixtures in N_2:

$$N_2O + h\nu \rightarrow N_2 + O(^1D) \quad (10)$$

$$O(^1D) + N_2 \rightarrow O(^3P) + N_2 \quad (11)$$

$$O(^3P) + CF_3I \rightarrow CF_3 + IO \quad (12a)$$

$$\rightarrow \text{products} \quad (12b)$$

$$O(^3P) + I_2 \rightarrow I + IO \quad (13)$$

CF_3I or I_2 was added upstream of the photolysis cell near the end of the flow tube, and N_2O was added with the main N_2 or He flow. Additional small flows of either He or N_2 were introduced right in front of the entrance and exit windows through which the photolysis laser beam was passed. This procedure, as mentioned earlier, minimized deposits on the windows. Without flush gases, solid deposits gradually formed on the windows. These flushes were <15% of the total gas flow. Due to the large flow velocity in the LIF reactor, the photolysis laser was passed through the photolysis cell along the axis of the flow to minimize loss of IO due to transport from the viewing region.

The IO temporal profiles were measured using a Nd:YAG pumped dye laser tuned to the band head of the $A^2\Pi_{3/2}$ ($v' = 2$) $\leftarrow$ $X^2\Pi_{3/2}$ ($v'' = 0$) transition at 444.8 nm, as described previously.[10] The dye laser beam intersected the photolysis laser at 90° at the center of the cell. Fluorescence was collected orthogonal to both laser beams by a convex lens (focal length of 5 cm), passed through a cutoff filter (λ > 475 nm) to discriminate against scattered light from the probe laser, and

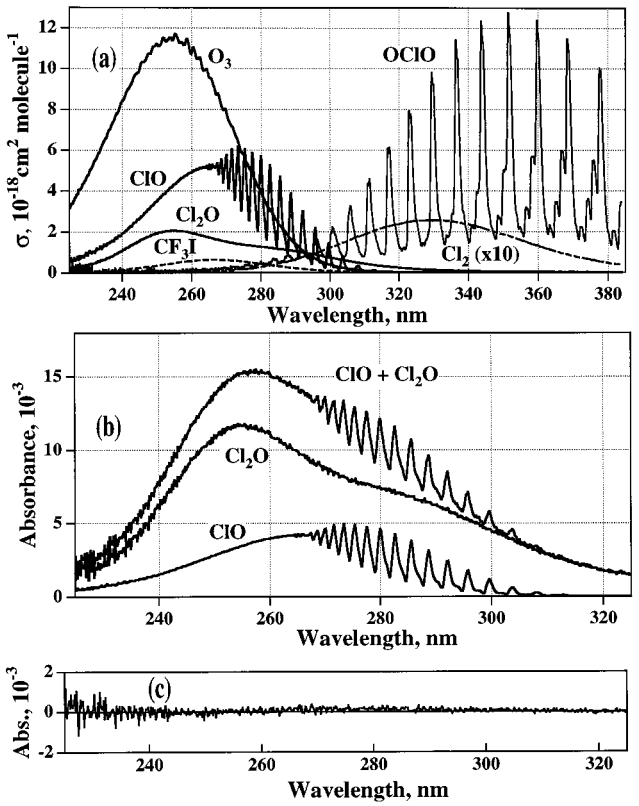

Figure 2. (a) Absorption spectra of species measured in the present study. Spectra are scaled to the absorption cross sections for each species as reported in ref 9. (b) Example of the absorption spectrum of ClO in an excess of Cl_2O at 298 K and the deconvolved ClO and Cl_2O spectra obtained after spectral subtraction of a ClO reference spectrum. (c) The residual shown was obtained by subtracting ClO, Cl_2O, and a small amount of Cl_2 from the spectrum labeled ClO + Cl_2O in (b).

imaged onto a photomultiplier tube (PMT). A second filter, which transmitted $\lambda < 600$ nm, was used to discriminate against an emission at wavelengths longer than 600 nm. This emission was present when the ClO source was on. The output of the PMT was sent to a gated charge integrator and microcomputer for analysis. The delay time between the photolysis and probe laser pulses was varied between 20 μs and 30 ms to obtain the temporal profile of IO. Even the shortest delay time of 20 μs allowed for thermalization and completion of any $O(^1D)$ reactions. Removal from the viewing zone of the reactor was nearly complete in 30 ms. The detection limit for IO, determined from $[N_2O]$ and laser fluence, was typically $\sim 1 \times 10^9$ molecule cm^{-3} (S/N = 1, averaging 100 laser shots).

The temperature in the photolysis cell, where the IO temporal profiles were measured, was regulated by flowing either cooled methanol or heated ethylene glycol from a thermostated bath through the jacket. The temperature at the intersection point of the photolysis and probe lasers was measured under flow and composition conditions, identical to those in which the IO temporal profiles were monitored by inserting a calibrated thermocouple through a movable tube located opposite the PMT. Because the pressures and fast flows were significantly different from the familiar discharge flow system, temperature gradients were of a concern. When N_2 was used as the bath gas, a large temperature gradient (up to 25 °C) between the solvent reservoir and the photolysis cell was observed. The use of He with ~1 Torr of N_2 added {to quench $O(^1D)$} nearly eliminated this gradient. The measured temperatures were found to be constant to ±2 K over this region.

Reagents. N_2 (UHP, >99.999%), He (UHP, >99.9999%), N_2O (UHP, 99.99%), and CF_3I (99%) were used without purification and were added to the reactor through calibrated electronic mass flow meters. Their concentrations were calculated using the flow rates and the total pressure, which was measured by a 50 Torr capacitance manometer. I_2 (99.8%) was introduced to the photolysis cell as a mixture in N_2. A small flow of N_2 was passed over I_2 crystals and the mixture passed through an absorption cell equipped to monitor 508 nm light from a Cd lamp ($\sigma = 2.5 \times 10^{-18}$ cm^2 $molecule^{-1}$).[14] This flow was then diluted by the main gas flow. The concentrations of N_2O, CF_3I, and I_2 are not essential for determining the IO + ClO rate coefficient. However, they are needed (along with the measured photolysis fluence) to estimate the concentration of IO to insure pseudo-first-order conditions and to estimate contributions of secondary reactions.

A mixture of 9.5% Cl_2/He (UHP, 99.9% Cl_2 in UHP He) was further diluted to <1% for generating Cl atoms, and its flow rate was measured using a mass flow meter. Cl_2O was synthesized as described previously[15] and stored at 195 K. Cl_2O was added to the reactor by bubbling a small flow of N_2 or He through the liquid. OClO was produced on-line by passing a small flow of the 9.5% Cl_2/He mixture over glass beads covered with sodium chlorite (80%). The Cl_2 to OClO conversion was nearly 100%. O_3 was produced by passing O_2 (UHP, 99.99%) through an ozonizer and trapping the O_3 on silica gel at 195 K. It was added to the flow tube by passing a flow of N_2 or He through the silica gel trap. Cl_2O, OClO, and O_3 were all measured by UV absorption along with ClO in the photolysis cell.

Results

ClO Generation. For measuring k_5, the total rate coefficient for reaction 5, ClO $\{(0.35-9.5) \times 10^{13}$ molecule $cm^{-3}\}$ was produced via reactions 6 or 7 with Cl_2O and OClO concentrations in excess ($[Cl_2O] = (5-14) \times 10^{13}$ and $[OClO] = (3-7) \times 10^{13}$ molecule cm^{-3}). IO was produced in a pulsed manner after ClO formation was complete to keep the concentration of Cl low ($[Cl] < 10^{10}$ atom cm^{-3}) and to suppress reactions of Cl with IO and its precursors:

$$Cl + IO \rightarrow ClO + I \quad (14)$$

$$Cl + I_2 \rightarrow ICl + I \quad (15)$$

$$Cl + CF_3I \rightarrow ICl + CF_3 \quad (16)$$

Bedjanian *et al.*[16] recently reported temperature independent rate coefficients of $k_{14} = (4.4 \pm 1.0) \times 10^{-11}$ cm^3 $molecule^{-1}$ s^{-1} and $k_{15} = (2.1 \pm 0.3) \times 10^{-10}$ cm^3 $molecule^{-1}$ s^{-1}, respectively. A rate coefficient of $k_{16}(T) = 6.25 \times 10^{-11} \exp[-1500/T]$ cm^3 $molecule^{-1}$ s^{-1} is also reported.[17] Excess Cl_2O and OClO also helped negate loss of ClO due to reactions 9a and 9c. With typical residence times of 15 and 20 ms in the flow tube and preliminary absorption cell, ClO loss due to its self-reaction was calculated to be <5% in these regions for the highest ClO concentrations used.

Within the photolysis cell, the typical residence time at 298 K was ~70 ms. During this time, the loss of ClO due to the bimolecular self-reaction was calculated to be <15% at 298 K. Since this loss was small, the average ClO concentration measured by UV absorption was nearly identical to the ClO concentration within the reaction zone, i.e. the middle of the photolysis cell. At low temperatures the bimolecular channels are greatly retarded; however, reaction 9d becomes faster. At 200 K and 5 Torr, the effective bimolecular rate coefficient for reaction 9d is $k_{9d} = 8.7 \times 10^{-15}$ cm^3 $molecule^{-1}$ s^{-1}.[9] Computer simulations showed that this rate coefficient results in a

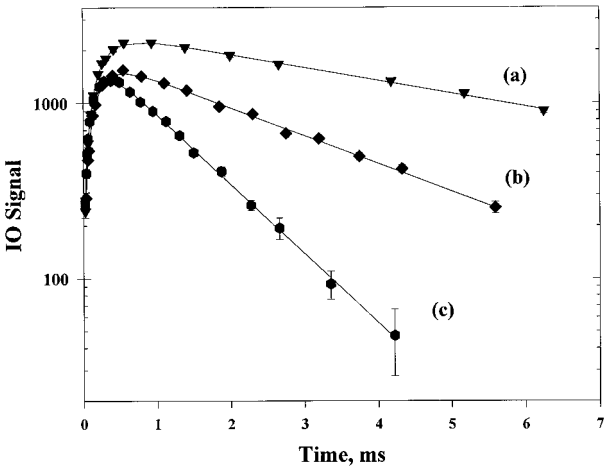

Figure 3. IO temporal profiles measured from the 193 nm photolysis of N_2O/CF_3I in an excess of ClO. ClO concentrations are (a) 0, (b) 1.68×10^{13}, and (c) 6.19×10^{13} molecule cm^{-3}. The solid lines are fits to eq V.

calculated ClO loss of ~6% in the temperature-controlled region at the highest [ClO] that was used. Note that approximately half of the total path length through the photolysis cell is in the temperature-controlled region; therefore, total losses due to reaction 9 are calculated to be <20% at the lowest temperatures and highest [ClO] studied. Although it is difficult to detect in the presence of excess Cl_2O, no evidence for Cl_2O_2 (ClO dimer) was observed in the UV absorption spectra taken at low temperatures suggesting that its formation was small. At high temperatures, the bimolecular channel leading to Cl_2 becomes the dominant loss of ClO; however, the total ClO loss was always calculated to be <20%.

OClO was used as the ClO precursor only at 298 K. At low temperatures OClO reacts[18] with ClO to form Cl_2O_3

$$ClO + OClO \xrightarrow{M} Cl_2O_3 \qquad (17)$$

resulting in a large ClO loss. Therefore, reaction 6 was the only ClO source used for low-temperature measurements.

IO Production. The 193 nm photolysis of N_2O/I_2 or N_2O/CF_3I was used to generate IO radicals via reactions 10−13. Because of the low vapor pressure of I_2 at $T < 250$ K, CF_3I was used as the IO source in the low-temperature experiments. The reaction of $O(^3P) + CF_3I$ is known to produce IO with ~85% yield with a rate coefficient of $k_{12}(T) = 7.9 \times 10^{-12} \exp[-175/T]$ cm^3 $molecule^{-1}$ s^{-1}.[19] Under typical experimental conditions ($[N_2O] = (1-5) \times 10^{15}$ molecule cm^{-3}, $[CF_3I] = (4-8) \times 10^{14}$ or $[I_2] = 5 \times 10^{13}$ molecule cm^{-3} and $E = (0.2-1.0)$ mJ $pulse^{-1}$ cm^{-2}), the IO signal reached a maximum value within 0.1−1 ms. A typical IO temporal profile in the absence of ClO is shown in Figure 3, curve a. The profile exhibits a fast exponential rise, reaction 12a, followed by a slower decay. The slow decay is due to pump out of the detection region and is described by

$$IO \rightarrow \text{loss} \qquad (18)$$

and the IO temporal profile can be described by the expression

$$[IO]_t = \frac{k_{12a}[CF_3I][O(^3P)]_0}{k_{18} - k'_a}(e^{-k'_a t} - e^{-k_{18}t}) \qquad (IV)$$

where $k'_a = k_{12}[CF_3I] + k_{19}$. Reaction 19

$$O(^3P) \rightarrow \text{loss} \qquad (19)$$

describes the loss of $O(^3P)$ atoms via transport out of the detection zone or reactions with impurities. The IO temporal profiles were fit to eq IV to obtain k'_a, at various concentrations of CF_3I. k_{12} was obtained from a linear least-squares fit of k'_a vs $[CF_3I]$ yielding a value of $k_{12}(298\ K) = 4.7 \times 10^{-12}$ cm^3 $molecule^{-1}$ s^{-1}, in good agreement with our recent results.[19] The intercept of the fit yielded a value of 1000 ± 150 s^{-1} for the loss of $O(^3P)$ via reaction 19.

The observed IO decays were exponential up to reaction times of 10−15 ms. The measured values of k_{18} ranged from 120 to 300 s^{-1} and were dependent upon the gas flow rate, pressure, and temperature. IO concentrations were calculated, using the known $[N_2O]$ and photolysis fluence, to be $< 3 \times 10^{11}$ molecule cm^{-3}. These low IO concentrations made the self-reaction of IO unimportant. The decay profiles of IO were strictly exponential and showed no evidence for a second-order loss process, as would be expected if the self-reaction of IO were occurring to a significant extent. Furthermore, variation of either $[N_2O]$ or the photolysis fluence over a factor of 5 did not affect the measured value of k_{18}, suggesting that the primary loss of IO was due to transport out of the reaction zone.

In 5−15 Torr of N_2, all of the $O(^1D)$ is quickly quenched to $O(^3P)$. However, when 4 Torr of He and 1 Torr of N_2 were used, up to 40% of the $O(^1D)$ reacted with N_2O to generate NO via

$$O(^1D) + N_2O \rightarrow N_2 + O_2 \qquad (20a)$$

$$\rightarrow 2NO \qquad (20b)$$

However, since the initial $[O(^1D)]$ was kept low, the NO produced was small and did not influence the IO temporal profile. As stated above, variation of the $[N_2O]$ (over a factor of 5), and consequently the concentration of photolytically produced NO, resulted in no measurable change in k_{18}. Therefore, the amounts of NO that were produced were insignificant.

IO + ClO Rate Coefficient. Initial tests were conducted to ensure that IO did not react with Cl_2, N_2O, or Cl_2O and that I atoms did not react with N_2O. Addition of Cl_2 (1×10^{15} molecule cm^{-3}) or Cl_2O (8×10^{14} molecule cm^{-3}) did not affect the IO temporal profile, and we place upper limits of $k_{21} < 2 \times 10^{-14}$ and $k_{22} < 3 \times 10^{-14}$ cm^3 $molecule^{-1}$ s^{-1} at 298 K for the reactions

$$IO + Cl_2 \rightarrow \text{products} \qquad (21)$$

$$IO + Cl_2O \rightarrow \text{products} \qquad (22)$$

Maintaining a constant [IO], varying the concentration of N_2O over a factor of 5 did not influence the IO temporal profile. The 351 nm photolysis of CH_2I_2 to produce I, in the presence of 35 Torr of N_2O, did not produce detectable concentrations of IO; on the basis of this observation, we place an upper limit of 1×10^{-18} cm^3 $molecule^{-1}$ s^{-1} for the reaction of $I + N_2O$ to produce IO. However, we did observe a reaction between IO and OClO

$$IO + OClO \rightarrow \text{products} \qquad (23)$$

The first-order rate constant for removal of IO in an excess of OClO yielded $k_{23} = (1.0 \pm 0.5) \times 10^{-13}$ cm^3 $molecule^{-1}$ s^{-1} in 5 Torr of N_2 at 298 K. Because this reaction is slow, we could still use low concentrations of [OClO] ($< 6 \times 10^{13}$ molecule cm^{-3}) to generate ClO and study reaction 5.

Cl_2O absorbs strongly at 193 nm, $\sigma(193) = 1.3 \times 10^{-18}$ cm^2 $molecule^{-1}$,[20] and the yield of Cl atoms has been measured to

be ~2;[21] therefore, the primary photodissociation channel for Cl_2O at 193 nm is

$$Cl_2O + h\nu \rightarrow 2Cl + O(^3P) \quad (24)$$

Therefore, O atoms produced by photolyzing Cl_2O {$(5-10) \times 10^{13}$ molecule cm^{-3}} were comparable to that from N_2O photolysis ($\sigma_{N_2O} = 9 \times 10^{-20}$ cm^2 $molecule^{-1}$).[3] As the Cl_2O concentration was increased, $[N_2O]$ was decreased so that the maximum IO signal was equal to or less than that observed in the absence of Cl_2O. In many cases, the N_2O was completely turned off and Cl_2O was used as the only source of $O(^3P)$. The Cl atoms produced by photolysis were rapidly consumed by Cl_2O to form ClO (reaction 6).

When IO was produced via reaction 12 in an excess of ClO, its temporal profile exhibited an initial exponential rise followed by an exponential decay (see Figure 3) due to the following reactions:

$$O(^3P) + CF_3I \rightarrow IO + CF_3 \quad (12a)$$

$$\rightarrow \text{products} \quad (12b)$$

$$O(^3P) + ClO \rightarrow O_2 + Cl \quad (25)$$

$$O(^3P) \rightarrow \text{loss} \quad (19)$$

$$IO + ClO \rightarrow \text{products} \quad (5)$$

$$IO \rightarrow \text{loss} \quad (18)$$

Note that any ClO lost due to reaction 25 will give ClO back rapidly via Cl reaction with the excess Cl_2O. This minimizes contributions to the IO loss rate due to Cl reacting with IO. The IO temporal profile in this mechanism is described by the expression:

$$[IO]_t = \frac{k_{12a}[CF_3I][O(^3P)]_0}{k'_d - k'_b}(e^{-k'_b t} - e^{-k'_d t}) \quad (V)$$

where $k'_b = k_{12}[CF_3I] + k_{25}[ClO] + k_{19}$ and $k'_d = k_5[ClO] + k_{18}$. The IO temporal profiles were fit by a nonlinear least-squares fitting routine to the equation $[IO]_t = A\{\exp(-k'_b) - \exp(-k'_d t)\}$ to determine both k'_b and k'_d. IO formation was always ~10 times faster than its decay due to reaction 5. Once the production of IO was complete, its temporal profile was governed by the equation

$$[IO]_t = [IO]_0 \exp(-k'_d t) \quad (VI)$$

Therefore, only the decay of IO was recorded in most of the measurements. When only the decay of IO was analyzed using eq VI, the k'_d obtained was within a few percent of that determined by analyzing the temporal profile using eq V. Reactions of CF_3 radicals could be problematic if they resulted in regeneration of IO. However, CF_3 most likely reacts with Cl_2 or Cl_2O in our system and, as shown by varying $[CF_3I]$ and photolysis fluence, does not affect the measured IO temporal profiles. The measured k'_d values were unaffected (<10%) by changes in $[Cl_2O]$, or [OClO], $[N_2O]$, $[CF_3I]$ and photolysis fluence over factors of 5 and were exponential over at least two 1/e lifetimes.

The temporal profiles of IO were measured at various [ClO], and k'_d versus [ClO] yielded the rate coefficient, k_5, as the slope (Figure 4a). Plots of k'_d versus [ClO] were linear over an order of magnitude in [ClO] with intercepts equal to the measured value of k_{18}. This observation, as well as the invariance of k'_d to changes in $[Cl_2O]$, $[CF_3I]$, and $[N_2O]$ indicate that IO loss was due solely to reaction with ClO and transport out of the reaction zone. These measurements were carried out at various temperatures between 200 and 360 K. In a few experiments at room temperature, k'_b, the appearance rate coefficient, was measured at various concentrations of ClO while holding the $[CF_3I]$ constant. From this appearance rate coefficient we obtained $k_{25}(298\ K) = (4.5 \pm 0.7) \times 10^{-11}$ cm^3 $molecule^{-1}$ s^{-1}.

The measured values of k_5 are summarized in Table 1 and shown as a function of temperature in Figure 5. The Arrhenius expression that describes the temperature dependence is $k_5(T) = (5.1 \pm 1.3) \times 10^{-12} \exp[(280 \pm 60)/T]$ cm^3 $molecule^{-1}$ s^{-1}, where the uncertainty represents 2σ precision from the Arrhenius plot. The estimation of the systematic error is described in the Discussion section.

IO + ClO Reaction Rate Coefficient in Excess O_3. Reaction 5 has many possible products, some of them leading to the formation of I atoms:

$$IO + ClO \rightarrow I + ClOO \quad (5a)$$

$$\rightarrow I + OClO \quad (5b)$$

$$\rightarrow ICl + O_2 \quad (5c)$$

$$\rightarrow OIO + Cl \quad (5d)$$

$$\rightarrow IOO + Cl \quad (5e)$$

$$\rightarrow I + Cl + O_2 \quad (5f)$$

$$\xrightarrow{M} IO_2Cl \quad (5g)$$

The reaction of I with ClO to produce IO is endothermic by ~8 kcal mol^{-1} and, hence, too slow to be important in this system. I atom production can be estimated in our experiments, albeit indirectly, by conversion of it back to IO via reaction 1. Under conditions where $k_1[O_3] \sim k_5[ClO]$, I atoms produced in reaction 5 regenerated IO at later times by reaction 1. ClO was generated by the $Cl + O_3$ reaction, and IO was generated by reaction 12 subsequent to photolytic production of O atoms from O_3. When the mixture of O_3 {$(1-10) \times 10^{14}$ molecule cm^{-3}}, ClO {$(1-8) \times 10^{13}$ molecule cm^{-3}}, and CF_3I (8×10^{14} molecule cm^{-3}) was photolyzed (0.3 mJ $pulse^{-1}$ cm^{-2}), the IO temporal profile showed a fast rise and then an exponential decay. However, at longer reaction times (>1 ms), reformation of IO was apparent (see Figure 6). The initial slope increased with [ClO], and the extent of IO regeneration increased with the O_3 concentration, as expected. The measured temporal profile of IO was fit using FACSIMILE, a nonlinear least-squares fitting routine,[22] to the mechanism described in Table 2. A total of 30 profiles were measured with varying [ClO] and $[O_3]$ ($[O_3]/[ClO] = 4-40$). The initial concentration of IO was calculated from the photolysis fluence, $[O_3]$, the absorption cross section for O_3 at 193 nm ($\sigma = 4.3 \times 10^{-19}$ cm^2 $molecule^{-1}$), and the net quantum yield for $O(^3P)$ in N_2 from O_3 photolysis at 193 nm.[9] These fits yielded a total rate coefficient of $k_5 = k_{5I} + k_{5nonI} = (1.37 \pm 0.26) \times 10^{-11}$ cm^3 $molecule^{-1}$ s^{-1}, in good agreement with our directly measured value (see Table 2 for definition of k_{5I} and k_{5nonI}). A rate constant for the channels which produce I atoms of $k_{5I} = (1.10 \pm 0.18) \times 10^{-11}$ cm^3 $molecule^{-1}$ s^{-1} was also obtained, which results in a yield of $\Phi(I) = 0.8 \pm 0.2$ for I atoms.

At higher $[O_3]$ all of the I atoms produced can be recycled rapidly relative to IO loss from reaction 5. Under these conditions decays of IO were exponential and varied linearly

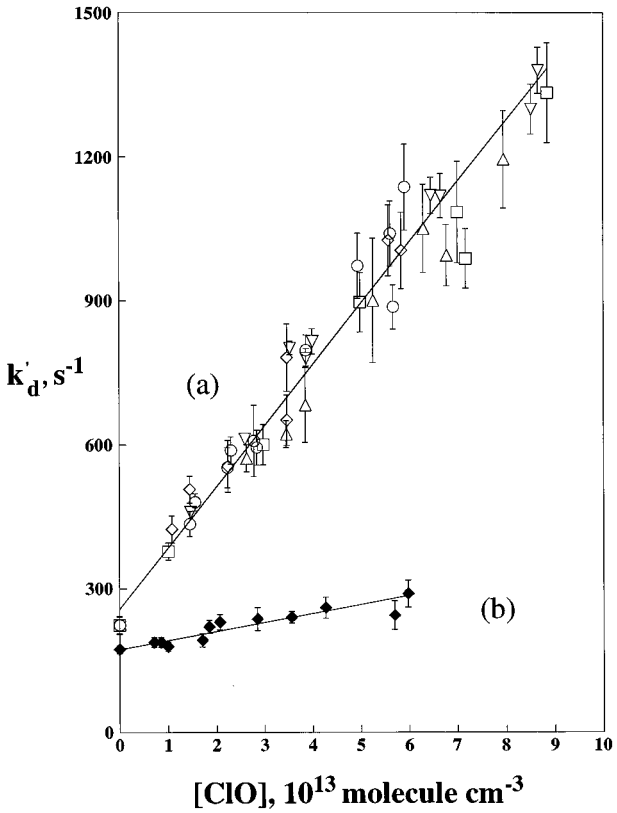

Figure 4. (a) Plot of k'_d vs [ClO] at 298 K. Symbols indicate different experimental conditions. Using Cl/Cl_2O and O/CF_3I radical sources, ○ ≡ 5 Torr of N_2; □ ≡ 4 Torr of He/1 Torr of N_2; ◇ ≡ 15 Torr of N_2. Using Cl/OClO and O/CF_3I radical sources, △; and using Cl/Cl_2O and O/I_2 radical sources, ▽ in 5 Torr of N_2. The various experiments are normalized to an average value for $k_{18} = 220$ s^{-1}. The line is the linear least-squares fit to the data. (b) A plot of k'_d vs [ClO] at 298 K (◆) in a large excess of O_3 ([O_3] = 4×10^{15} molecule cm^{-3}). The line is the least-squares fit to the data.

TABLE 1: Summary of the Rate Coefficients Measured for the IO + ClO Reaction

T (K)	P_{tot} (Torr)	L_{eff} (cm)	[ClO] (10^{13} molecule cm^{-3})	($k_5 \pm 2\sigma$)[a,b] (10^{-11} cm^3 $molecule^{-1}$ s^{-1})
362	5.3	36.5 ± 0.2	1.1−6.4	1.03 ± 0.08
326	5.3	35.4 ± 0.2	0.6−7.6	1.26 ± 0.05
298	5.4	32.6 ± 0.4	1.4−8.8	1.17 ± 0.08[c]
	5.1	32.6 ± 0.4	2.6−9.6	1.16 ± 0.07[d]
	5.1	34.1 ± 0.3	1.4−8.2	1.47 ± 0.07[e]
	5.3	34.1 ± 0.3	1.0−8.9	1.20 ± 0.15
	15.3	34.1 ± 0.3	1.1−5.9	1.43 ± 0.18[e]
				avg at 298 K = 1.29 ± 0.27
269	5.2	32.7 ± 0.5	0.7−8.4	1.47 ± 0.10
249	5.1	32.4 ± 0.6	0.5−7.0	1.64 ± 0.12
243	5.3	31.0 ± 0.3	0.7−6.8	1.84 ± 0.13
226	5.2	30.1 ± 0.5	0.4−5.3	1.94 ± 0.13
213	5.1	30.2 ± 0.4	0.7−6.7	1.91 ± 0.17
210	16.0	30.2 ± 0.4	1.2−5.8	1.94 ± 0.12
200	5.3	29.1 ± 0.7	0.5−7.3	2.00 ± 0.15

[a] Uncertainties are from the precision of the k'_d vs [ClO] fit. [b] Unless otherwise noted, measurements were made using ≈4 Torr of He and 1 Torr of N_2 and using O + CF_3I to produce IO and Cl + Cl_2O to produce ClO. [c] Using O + I_2 reaction as the IO source in N_2. [d] Using Cl + OClO as the ClO source in N_2. [e] In N_2.

with [ClO], and the IO temporal profile was described by eq VI where $k'_d = (k_{5nonI}[ClO] + k_{18})$. ClO and IO were produced via reactions 8 and 12 as in the previous experiments. The photolysis fluence was maintained at a low level (0.02 mJ $pulse^{-1}$ cm^{-2}) to avoid producing too much IO at these high concentrations of O_3 ([O_3] = 4×10^{15} molecule cm^{-3}). A plot

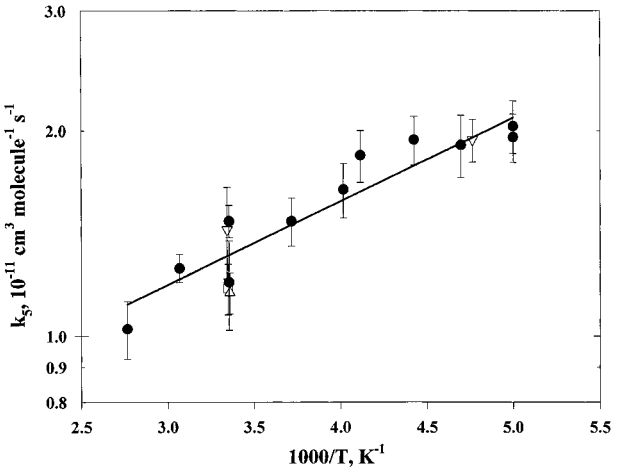

Figure 5. Variation of the measured rate coefficient, k_5, with temperature. Symbols are Cl/Cl_2O and O/CF_3I radical sources at 5 Torr (●) and 15 Torr (▽). Cl/OClO and O/CF_3I radical sources (△), Cl/Cl_2O and O/I_2 radical sources (□). The line is an Arrhenius fit yielding $k_5(T) = (5.1 \pm 1.7) \times 10^{-12}$ exp[(280 ± 80)/T] cm^3 $molecule^{-1}$ s^{-1}. The uncertainty includes 2σ uncertainty from the fit and 18% estimated systematic error.

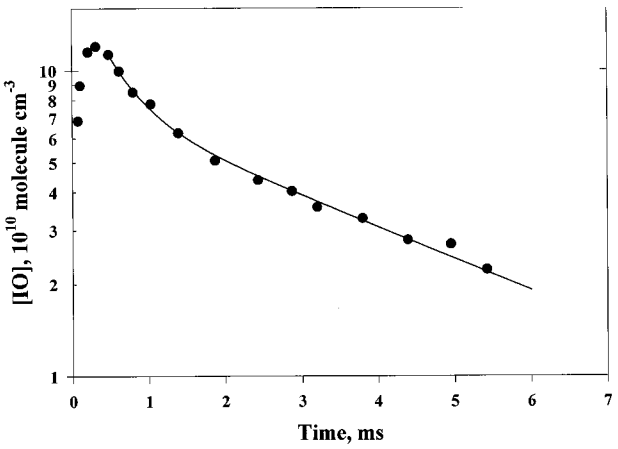

Figure 6. Temporal profile of IO in an excess of O_3 ([O_3] = 7.5×10^{14} molecule cm^{-3}) and ClO ([ClO] = 9.2×10^{13} molecule cm^{-3}). The line is the fit to the data using the mechanism described in Table 2 and gives a rate coefficient of $k_5 = 1.4 \times 10^{-11}$ cm^3 $molecule^{-1}$ s^{-1} and a yield of 0.8 for I atom production.

TABLE 2: Reaction Mechanism Used To Determine the Yield of I Atoms from Reaction 5

reaction		k(298 K)[a]	notes
IO + ClO → I + products	(5)	k_{5I}	varied in fit
IO + ClO → non-I products	(5)	k_{5nonI}	varied in fit
I + O_3 → IO + O_2	(1)	1.2×10^{-12}	*b*
Cl + O_3 → ClO + O_2	(8)	1.2×10^{-11}	*c*
IO → loss	(18)	150	measured
I → loss	(27)	150	*d*

[a] Units of cm^3 $molecule^{-1}$ s^{-1} for second-order reactions and s^{-1} for first-order reactions. [b] From ref 9. [c] From ref 10. [d] Assumed to be the same as for IO.

of k'_d vs [ClO] from this experiment is shown in Figure 4, curve b, and yields a rate coefficient for $k_{5nonI} = (1.88 \pm 0.36) \times 10^{-12}$ cm^3 $molecule^{-1}$ s^{-1}. Combining this with the total rate coefficient, k_5, (Figure 4, line a), gives a branching ratio of $\Phi = 0.14 \pm 0.04$ at 298 K for the sum of channels that do not produce I atoms.

These measurements were also attempted at 223 K. However, due to the slower rate coefficient for the I + O_3 reaction, we were unable to attain conditions where $k_1[O_3] > 10k_5[ClO]$ and

measure [ClO] and changes in the IO loss. Therefore, we had to rely on modeling the measured temporal profile of IO to obtain information on the yield of I atoms. From 10 temporal profiles ($[O_3] = 1 \times 10^{15}$, $[ClO] = (1-8) \times 10^{13}$ molecule cm^{-3}), we obtained a yield of $\Phi(I) = 0.78 \pm 0.25$ for I atom production from FACSIMILE simulations. Although the uncertainties are larger than at 298 K, it appears that the I atom yield does not change significantly with temperature.

Discussion

The measured values of k_5 are listed in Table 1. These values were insensitive to variation of [N_2O], [CF_3I], [Cl_2O], [OClO] and varying the photolysis fluence over a factor of 5. The 298 K value of k_5 was the same using different chemical sources for both IO and ClO. These observations strongly indicate that IO was reacting solely with ClO and its decay was not influenced by reactions with other precursors or radicals. If reaction 5 produced I*, electronically excited I atoms, its reaction with ClO is likely to produce IO and is likely to be rapid. However, on the basis of known thermochemistry, reaction 5 cannot lead to I*.

The accuracy of our rate coefficients are critically dependent upon the accuracy of the ClO concentration in the volume where IO temporal profiles are measured. The major contributions to this uncertainty are the possible loss of ClO along the length of the reactor and inaccuracies in the optical measurements. We measure the ClO column in the absorption cell while the IO temporal profile is controlled by ClO concentration in the reaction zone. As discussed above, under all experimental conditions, losses due to the ClO self-reaction are calculated to be <20% and computer simulations of the ClO loss along the absorption path length indicated that the measured average [ClO] is representative of the [ClO] in the reaction zone to within ±5% even at the highest [ClO].

Several experimental tests were carried out to verify the above calculations of [ClO]: (1) We added absorption cells (with an glass insert to cover the O-rings) to measure [ClO] upstream and downstream of the photolysis cell. The value of k_5 determined at 298 K when [ClO] was measured using a 50 cm absorption cell upstream of the LIF reactor was $k_5 = (1.1 \pm 0.1) \times 10^{-11}$ cm^3 $molecule^{-1}$ s^{-1}. When the absorption cell was placed downstream of the photolysis cell, we measured $k_5 = (1.7 \pm 0.2) \times 10^{-11}$ cm^3 $molecule^{-1}$ s^{-1}. These values bracket the rate coefficient obtained by measuring [ClO] directly through the LIF reactor. The loss of ClO necessary to reproduce these numbers is consistent with the ClO + ClO reaction being the main loss process. (2) The rate coefficient for the O + ClO reaction was measured by following the IO rise to be $k_{25} = (4.5 \pm 0.7) \times 10^{-11}$ cm^3 $molecule^{-1}$ s^{-1}, which is within 15% of the recommended value.[9] (3) We used OClO as the ClO precursor, with OClO in excess. Since each Cl atom, produced via the ClO self-reaction, reacts with OClO to generate 2ClO, the removal of ClO via reactions 9a, 9b, and 9c collectively replenish the ClO that was lost. This process effectively eliminates depletion of ClO via reaction 9. The rate coefficient measured using the OClO source agreed with that measured using the Cl_2O source. (4) Since reaction 9 is second-order, the loss of ClO should increase as $[ClO]^2$ at larger concentrations. If this loss was significant, the fractional loss of ClO should be larger and display curvature in the k'_d vs [ClO] plots. As mentioned earlier, the plots of k'_d vs [ClO] were linear in all experiments. From these observations and the computer simulations, we estimate that the uncertainty in the measured [ClO] within the reaction zone due to losses was ≈±5% via the self-reaction and the first-order wall loss.

Other sources of systematic error include the spectral subtractions and the absorption cross section for ClO at 253.7 nm. Spectral subtractions of ClO from the excess Cl_2O were reproducible at the ±2% level, and the combined uncertainty in the absorption cross section and the effective path length for the [ClO] measurements is estimated to be <±10%. Another small source of systematic error involves the measurement of the reaction zone temperature ±2%, which gives an uncertainty of ±1% in [ClO]. Therefore, our total systematic error in k_5 is ±18%. On the basis of these values we quote $k_5 = (5.1 \pm 1.7) \times 10^{-12} \exp[(280 \pm 80)/T]$.

We can place the measured value of k_5 in the context of other analogous reactions of halogen monoxides.[9,23] The IO + ClO reaction exhibits a weak negative temperature dependence ($E/R = -280$ K^{-1}). The reactions of halogen oxides with other halogen oxides are thought to occur via the formation of an intermediate complex (XOOY or OXOY), which can then be stabilized or decompose to form products. The competition between decomposition of the complex back to reactants or to products or stabilization leads to the observed increase in the rate coefficient at lower temperatures.

The room temperature rate coefficient and activation energy for reaction 5 are remarkably similar to that for the reaction between ClO and BrO,[24-28] $k_{27}(298) = 1.2 \times 10^{-11}$ cm^3 $molecule^{-1}$ s^{-1}, $E/R \approx -300$ K.

$$BrO + ClO \rightarrow Br + ClOO \qquad \Phi \approx 0.4 \qquad (27a)$$

$$\rightarrow Br + OClO \qquad \Phi \approx 0.5 \qquad (27b)$$

$$\rightarrow BrCl + O_2 \qquad \Phi \approx 0.1 \qquad (27c)$$

The BrO + ClO reaction is known to proceed through three different channels,[25-28] whose branching ratios change with temperature. The IO + ClO reaction can also proceed through analogous pathways. Reaction 5a, 5b, and 5c are exothermic by 4.6, 5.3, and 49.1 kcal mol^{-1}, respectively at 298 K, using a $\Delta_f H°(298\ K)(IO) < 28.8$ kcal mol^{-1}.[19] Reaction 5f is slightly endothermic but highly favored entropically. The thermochemistry of channels 5d, 5e, and 5g are unknown due to the lack of thermochemical data on OIO, IOO, and IO_2Cl. ClOO is known to be weakly bound (∼5 kcal mol^{-1})[9] and will rapidly decompose to Cl and O_2. On the basis of trends in the halogen species, IOO is predicted to be less stable than ClOO;[29,30] therefore, channels 5a and 5e effectively result in the production of atomic chlorine and iodine (channel 5f).

Experiments in excess O_3 indicated that I atoms were a major product in this reaction. At 298 K and 7 Torr of N_2, a yield of 0.14 ± 0.04 was measured for the sum of channels that do not produce I atoms ($\Phi(nonI) = \{k_{5c} + k_{5d} + k_{5g}\}/k_5$). By comparison with other halogen monoxide reactions, channel 5c is the most probable pathway.[9] The analogous BrCl formation from reaction 27 has been observed[25-27] to have a yield of ≈10%. It is possible that electronically excited ICl could be formed and dissociate at the low pressures utilized here. At higher pressures, quenching of ICl* could compete with dissociation and, possibly, increase the branching ratio for this channel. Toohey *et al.*[24] have suggested a similar mechanism in the BrO + ClO reaction to explain their observed decreases in the branching ratio of Br with increasing pressure. A complete pressure dependence of the branching ratio and/or detection of ICl is necessary to better understand the mechanism of the IO + ClO reaction.

Formation of OIO, which has been recently observed by flash photolysis of an I_2/O_3 mixture,[31] cannot be ruled out, but a recent estimation of the enthalpy of formation of this radical ($\Delta_f H =$

40 kcal mol^{-1})[32] suggests that this channel would be ≈13 kcal mol^{-1} endothermic and, thus, unimportant. The lack of any pressure dependence in the rate coefficient also suggests that stabilization of $IClO_2$ is not important in our system. However, all of our measurements were done at <15 Torr; therefore, this species cannot be completely ruled out at higher pressures. Mauldin *et al.*[30] observed an unknown product in the BrO + BrO reaction at 223 K and 300 Torr N_2 and tentatively identified it as Br_2O_2. Similar observations have been reported suggesting that formation of $IClO_2$ may also be possible.[33]

Our experiments cannot distinguish between channels 5b and the channels that produce atomic I and Cl. In the atmosphere, the production of I + OClO in reaction 5 will not lead to a net ozone loss. We attempted to monitor OClO by LIF; however, our detection sensitivity was an order of magnitude too poor to observe the concentrations of OClO that could be produced under our experimental conditions.

Atmospheric Implications. The modeling study of Solomon *et al.*[8] assumed $k_5 = 1 \times 10^{-10}$ cm^3 $molecule^{-1}$ s^{-1}. Using this rate coefficient, a total iodine abundance of 1 pptv in the stratosphere was necessary to completely account for the observed trend in low-altitude, midlatitude O_3 loss during the past two decades. Our measured value at temperatures characteristic of the stratosphere is approximately a factor of 5 lower than the assumed value. Thus, the interaction of iodine with chlorine will be five times less efficient at destroying ozone than predicted if we assume reaction 5 does not produce OClO. The contribution of this reaction to stratospheric ozone loss is discussed in detail in the next paper.

Note Added in Proof. Yuri Bedjanian, Georges Le Bras and Gilles Poulet have measured the 298 K rate coefficient k_5(298 K) = (1.1 ± 0.2) × 10^{-11} cm^3 $molecule^{-1}$ s^{-1} using a mass spectrometric discharge flow system (*J. Phys. Chem. A* **1997**, *101*, 4088). They also report branching ratios of (0.55 ± 0.03), (0.25 ± 0.02), and (0.20 ± 0.02) for channels 5b, 5f, and 5c, respectively. These results are in excellent agreement with those reported in this paper.

Acknowledgment. The authors thank Dr. S. Solomon for useful discussions concerning this work. We also acknowledge Dr. Bedjanian for both sending us preprints prior to publication and his insightful comments. This work was funded in part by NASA's Mission to Planet Earth Program through the Upper Atmospheric Research Program.

References and Notes

(1) Reifenhauser, W.; Heumann, K. G. *Atmos. Environ.* **1992**, *26A*, 2905.

(2) Klick, S.; Abrahamsson, K. *J. Geophys. Res.* **1992**, *97*, 12683.

(3) Moyers, J. L.; Duce, R. A. *J. Geophys. Res.* **1972**, *77*, 5229.

(4) Zafiriou, O. C. *J. Geophys. Res.* **1974**, *79*, 2730.

(5) Chameides, W. L.; Davis, D. D. *J. Geophys. Res.* **1980**, *85*, 7383.

(6) Barrie, L. A.; Bottenheim, J. W.; Hart, W. R. *J. Geophys. Res.* **1994**, *99*, 25313.

(7) *The Tropospheric Chemistry of Ozone in the Polar Regions*, Proceedings of the NATO Advanced Research Workshop; Niki, H., Becker, H. B., Eds.; Springer-Verlag: New York, 1993.

(8) Solomon, S.; Garcia, R. R.; Ravishankara, A. R. *J. Geophys. Res.* **1994**, *99*, 20491.

(9) DeMore, W. B.; Sander, S. P.; Golden, D. M.; Hampson, R. F.; Kurylo, M. J.; Howard, C. J.; Ravishankara, A. R.; Kolb, C. E.; Molina, M. J. *Chemical Kinetics and Photochemical Data for Use in Stratospheric Modeling, Evaluation No. 11*; Jet Propulsion Laboratory: Pasadena, CA, 1994.

(10) Turnipseed, A. A.; Gilles, M. K.; Burkholder, J. B.; Ravishankara, A. R. *Chem. Phys. Lett.* **1995**, *242*, 427.

(11) Trolier, M.; Mauldin, R. L., III; Ravishankara, A. R. *J. Phys. Chem.* **1990**, *94*, 4896.

(12) Molina, L. T.; Molina, M. J. *J. Geophys. Res.* **1986**, *91*, 14501.

(13) Solomon, S.; Burkholder, J. B.; Ravishankara, A. R.; Garcia, R. R. *J. Geophys. Res.* **1994**, *99*, 20929.

(14) Calvert, J. G.; Pitts, J. N., Jr. *Photochemistry*; Wiley: New York, 1966.

(15) Renard, J. J.; Bolker, H. I. *Chem. Rev.* **1976**, *76*, 487.

(16) Bedjanian, Y.; LeBras, G.; Poulet, G. *J. Phys. Chem.* **1996**, *100*, 15130.

(17) Kaiser, E. W.; Wallington, T. J.; Hurley, M. D. *Int. J. Chem. Kinet.* **1995**, *27*, 205.

(18) Burkholder, J. B.; Mauldin, R. L., III; Yokelson, R. J.; Ravishankara, A. R. *J. Phys. Chem.* **1993**, *97*, 7597.

(19) Gilles, M. K.; Turnipseed, A. A.; Talukdar, R. K.; Rudich, Y.; Villalta, P. W.; Huey, L. G.; Burkholder, J. B.; Ravishankara, A. R. *J. Phys. Chem.* **1996**, *100*, 14005.

(20) Lin, C. L. *J. Chem. Eng. Data* **1976**, *21*, 411.

(21) Gilles, M. K.; Ravishankara, A. R. Unpublished data.

(22) Malleson, A. M.; Kellett, H. M.; Myhill, R. G.; Sweetenham, W. P. *FACSIMILE*; A. E. R. E. Harwell Publications Office: Oxfordshire, 1990.

(23) Sander, S. P. *J. Phys. Chem.* **1986**, *90*, 2194.

(24) Toohey, D. W.; Anderson, J. G. *J. Phys. Chem.* **1988**, *92*, 1705.

(25) Turnipseed, A. A.; Birks, J. W.; Calvert, J. G. *J. Phys. Chem.* **1991**, *95*, 4356.

(26) Friedl, R. R.; Sander, S. P. *J. Phys. Chem.* **1989**, *93*, 4756.

(27) Poulet, G.; Lancar, I. T.; Laverdet, G.; LeBras, G. *J. Phys. Chem.* **1990**, *94*, 278.

(28) Sander, S. P.; Friedl, R. R. *J. Phys. Chem.* **1989**, *93*, 4764.

(29) Blake, J. A.; Browne, R. J.; Burns, G. J. *J. Chem. Phys.* **1970**, *53*, 3320.

(30) Mauldin, R. L., III; Wahner, A.; Ravishankara, A. R. *J. Phys. Chem.* **1993**, *97*, 7585.

(31) Himmelmann, S.; Orphal, J.; Bovensmann, H.; Richter, A.; Ladstaetter-Weissenmayer, A.; Burrows, J. P. *Chem. Phys. Lett.* **1996**, *251*, 330.

(32) Chase, M. W. *J. Phys. Chem. Ref. Data* **1996**, *25*, 1297.

(33) Johnsson, K.; Engdahl, A.; Koelm, J.; Nieminen, J.; Nelander, B. *J. Phys. Chem.* **1995**, *99*, 3902.